MAGNETIC FIELD OBSERVATIONS ON DE-A AND -B

W. H. FARTHING, M. SUGIURA, and B. G. LEDLEY
Goddard Space Flight Center, Greenbelt, Maryland 20771, U.S.A.

and

L. J. CAHILL, Jr.
University of Minnesota, Minneapolis, Minnesota 55455, U.S.A.

(Received 11 May, 1981)

Abstract. Magnetic field observations are conducted on each of the DE-A and -B satellites by a triaxial fluxgate magnetometer. In the basic mode the instrumental resolution is ± 1.5 nT; in addition, the DE-A magnetometer has two modes of higher resolution: ± 0.25 nT and ± 20 pT. The sampling rate is 16 vector samples per second in all modes. The experiment objectives include observations of field-aligned currents, magnetospheric equatorial currents, and ULF waves. These observations, taking full advantage of the specifically selected orbits of the two spacecraft and of the unique combination of instruments, are performed to achieve a better understanding of the electrodynamic coupling within the atmosphere-ionosphere-magnetosphere system and of wave-particle interactions which contribute to the coupling processes.

1. Introduction

In the electrodynamic coupling processes within the magnetosphere-ionosphere-atmosphere system, electric currents play a fundamental role. The Joule heating by ionospheric currents constitutes a significant heat source that influences the dynamics of the thermosphere. Because of the high electrical conductivity parallel to the magnetic field, field-aligned currents provide a rapid and efficient means of transporting energy between the distant regions of the magnetosphere and the ionosphere that are linked by the magnetic field lines. The processes through which this energy transfer is accomplished may involve a significant transport of charged particles between the magnetosphere and the ionosphere. The magnetospheric equatorial currents, which are intimately related to the dynamics of the plasma and energetic charged particles in the magnetosphere, appreciably distort the geomagnetic field. Magnetic fields and currents also play a role in plasma instabilities in which fields and particles exchange energy. Therefore the magnetic field observations from the Dynamics Explorer (DE)-A and -B satellites constitute an important element of the mission. In particular, simultaneous observations of magnetic fields at low and high altitudes, combined with measurements of other physical parameters, highlight the uniqueness of the mission.

2. Objectives

Deduction of field-aligned currents from the magnetic field observations with high resolution on DE-A and -B is one of the most important objectives of the magnetometer experiments. The low altitude (DE-B) magnetic field observations will provide the most dependable means of detecting field-aligned currents. A comparison of the DE-B

Space Science Instrumentation **5** (1981) 551–560. 0377–7936/81/0054–0551 $01.50.

magnetometer data with measurements of precipitated charged particles will yield information on the current carriers. Combined with the electric field measurements and with the ionospheric conductivity distribution deduced from the particle measurements, the magnetometer data will allow the construction of a model for the field-aligned currents. When the orbit of DE-A is along a magnetic flux tube that, at low altitudes, contains DE-B, a unique opportunity exists to investigate the current continuity, the current carriers, and the mechanisms that drive the field-aligned currents. In such a study the auroral images and particle measurements on DE-A will be indispensable elements. The combination of field-aligned current measurements (together with those of other electrodynamical parameters) and neutral atmosphere observations such as neutral wind observations will provide a new opportunity for investigating the processes of the atmosphere-magnetosphere coupling.

The magnetospheric equatorial current, often referred to as the ring current, is receiving renewed interest because of the recent observations that suggest a significant contribution by heavy ions of ionospheric origin. Not only is the composition of the particles contributing to the magnetospheric equatorial current inadequately known, the very processes that give rise to the current are not completely understood. These unsolved problems will be studied with data obtained by the DE instruments.

The DE-A magnetometer experiment is also well suited for the study of ultra low frequency (ULF) waves. Investigation of these waves is important in the DE mission because they contribute to the exchange of energy, from particles to waves and from the magnetosphere to the ionosphere. With observations of waves in the lower frequency range, 0.01 to 0.001 Hz, we will investigate resonant oscillations of magnetic shells in the magnetosphere. Observations of waves in the higher frequency range of the magnetometer, 0.2 to 5.0 Hz, will enable us to study the wave-particle interactions by ion cyclotron resonance. The orbit of DE-A, traveling in a magnetic flux tube for 1000 to 2000 km, will offer the first opportunity to investigate the details of these macroscopic and microscopic plasma resonance processes.

3. Instrument Description

3.1. Fluxgate sensor

The DE magnetometers are triaxial fluxgate sensors. When a saturable core immersed in an ambient magnetic field is driven into alternating positive and negative saturation, a flux component at the second harmonic of the drive frequency is induced by the ambient field. This flux, which is proportional to the magnitude of the field, is sensed, synchronously detected, integrated, and fed back to the sensing coil, wound solenoidally about the core sample. The coil axis defines the direction of sensitivity for that magnetic axis and the field generated by the feedback current nulls the ambient field in that direction. A closed loop system is formed in which the sensitivity and stability are determined primarily by the value and stability of the feedback transfer function, which

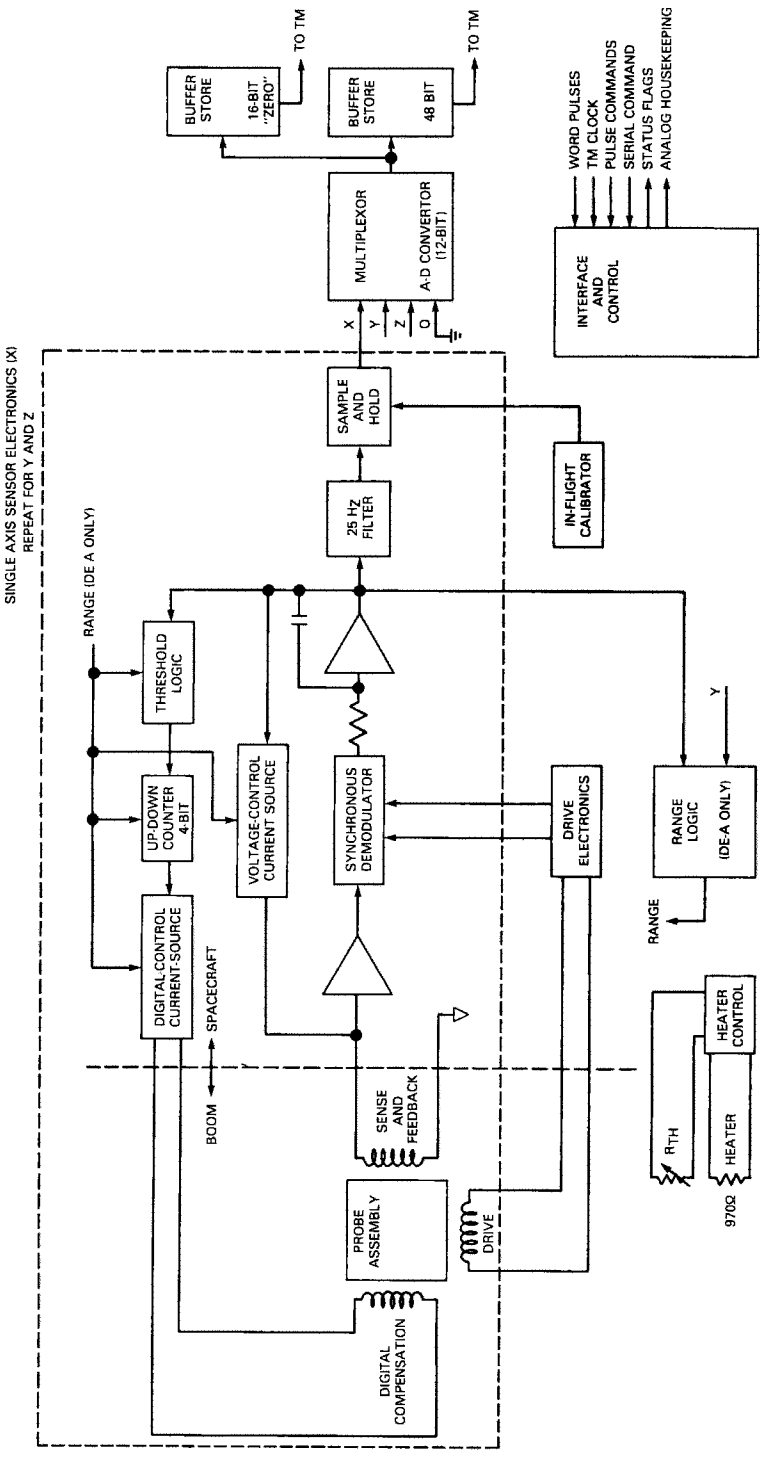

Fig. 1. Magnetometer block diagram. The single axis electronics are repeated for the y and z axes, and can be treated as a first order servo loop nulling the field along the sensitive axes for its corresponding probe.

includes a voltage-to-current transducer and the solenoidal coil constant. Figure 1 presents a block diagram describing the magnetometer system.

The theory of the fluxgate mechanism has been amply presented in the literature [1–4]. It suffices to stay that of the various geometries which have been used for fluxgate magnetometers, the DE instruments are of the ring core type. In this construction, the core sample is formed by winding a few turns of permalloy tape onto a disc shaped bobbin (one inch in diam), and the drive winding is toroidal about the core sample. The core assembly is then epoxied into a rectangular coil form which supports the solenoidal coil serving both sensing and feedback functions. In this instrument, a separate coil is wound coaxially with the sense coil, as described later, to extend the dynamic range. The probe structure is shown in Figure 2. For the bobbin, inconel X-750 [5] was chosen for magnetic properties, weldability and thermal match to the permalloy core material. The coil form is made of graphite fiber reinforced plastic because of its low temperature coefficient.

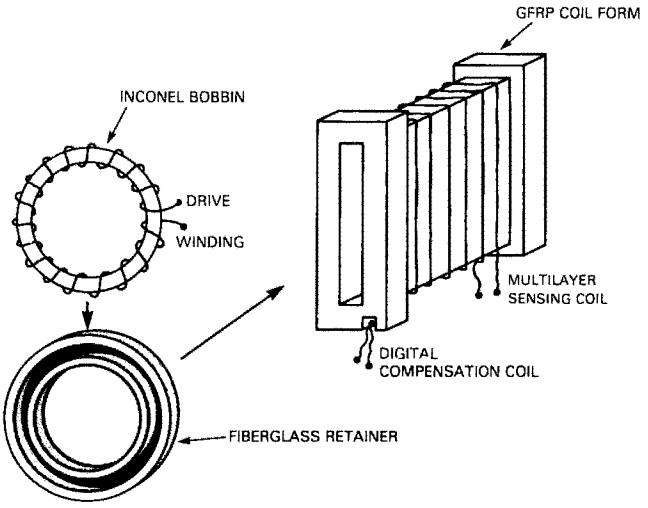

Fig. 2. Probe structure. The inconel bobbin is put in the retainer, which is then epoxied into the graphite fiber reinforced plastic (GFRP) coil form.

The ring core geometry is superior to other geometries which have been used concerning the noise level and the zero offset performance. It has disadvantages in that the dimension of the gradient-free field region along the sensitive axis relative to the effective length is smaller than is the case for geometries in which the sample is elongated along the sensitive axis. The ring core geometry also leads to higher induced fields transverse to the sensitive axis which couple more strongly into the other two axes of a triaxial sensor. Both of these effects require the use of stable materials in the fabrication of the sensor. In the DE magnetometer, graphite fiber reinforced plastic is used as the primary structural element to take advantage of its superior thermal stability. The cross coupling effect is controlled by spacing the individual sensors approximately 15 cm apart and by including the residual effects as linear modifications to the instrument calibration.

In practice, an optical cube is mounted to the sensor structure, and the direction and sensitivity of each effective axis are determined by exposure in the Goddard Space Flight Center Magnetic Test Facility to fields generated along the cube faces. A matrix is thereby determined which transforms measurements in the effective sensor axes to the orthogonal system of the optical cube. This procedure automatically includes linear cross coupling terms whose effect is to modify the direction and sensitivity of a single probe from its performance in the absence of interfering fields.

3.2. Electronics

The approach used to obtain the ± 1.5 nT resolution and $\pm 62\,000$ nT dynamic range desired for the DE instruments is illustrated schematically in Figure 1. The dynamic range of the fluxgate sensor is set by the voltage controlled current source to nominally ± 6000 nT, corresponding to an output voltage of ± 5 V. The dynamic range is extended to the $\pm 62\,000$ nT required for the DE mission by a precision 4 bit digitally controlled current source which generates compensation fields in increments of nominally 8000 nT from $-56\,000$ to $+56\,000$ nT. Separate solenoidal coils are used for the digital compensation. The up-down counter maintains the sum of the ambient and digital compensation fields within the ± 6000 nT dynamic range of the analog feedback loop.

The analog outputs of each axis are band limited and multiplexed through simultaneous sample and hold circuits into a 12 bit analog-to-digital (A-D) converter. The 4 bit digital current source and the 12 bit A-D output for each axis are strobed into a 48 bit output buffer and held for transfer to the spacecraft telemetry stream.

The conversion sequence is started at the completion of transfer of the last 8 bits of magnetometer data in a sample. All analog data are simultaneously 'held' by the sample-and-hold circuits and the x, y, and z outputs are sequenced through the A-D converter and loaded into the output buffer. Finally, signal ground is gated to the A-D converter and the output stored in a separate buffer to monitor the zero offset of the converter. The vector data are transferred to the telemetry stream 16 times per second. The zero offset data are taken once each 4 s by the spacecraft subcommutator.

An in-flight calibration mode is available on command. It sequences near full scale positive and negative voltage levels as well as zero reference through the sample-and-hold circuits thereby monitoring the A-D converter functional operation and the zero offset stability of the sample-and-hold circuits. The analog sensitivity of each axis will be monitored in a relative sense through the recurring steps of current applied from the digital current source. Absolute calibrations are not possible since the two solenoidal coils have approximately the same temperature coefficient.

3.3. Thermal control

Even with the use of graphite fiber reinforced plastic, the sensitivity of the sensors has a temperature dependence amounting approximately to 3×10^{-5} nT/nT-°C. This thermal effect is calibrated and taken into account in the data processing. Since temperature variations in orbit could still prove troublesome, a thermostatically controlled heater is incorporated to control the sensor temperature. The heater is driven by

the spacecraft unregulated bus so that it can be left on between data acquisition periods on the power limited spacecraft. Ground tests indicated that temperature control can be maintained with about 0.6 W average power for all but the most extreme environments to be encountered over the DE lifetime.

3.4. High resolution modes

The DE-A spacecraft, with its apogee near 5 R_E, will spend much of its time in low field regions where the 62 000 nT dynamic range is not required. These are also the regions in which magnetic pulsations and other wave phenomena occur. Description of such wave phenomena requires higher resolution than the ± 1.5 nT provided by the basic mode. For this reason the magnetometer for DE-A incorporates two higher resolution modes. In one of these the sensors auto-range to a ± 1000 nT mode and the current source is disabled. The resulting resolution is ± 0.25 nT. In the other high resolution mode the sensors auto-range to a range of ± 80 nT and the current source provides compensation fields in steps of 110 nT. At the resolution of ± 0.020 nT, or ± 20 pT obtained in this mode, the instrument and spacecraft noise become a significant factor. Spectral analysis techniques will be used to search for low frequency wave phenomena riding above the noise spectrum. Ground commands configure the instrument to either inhibit auto-ranging or to enable auto-ranging to one of the available high resolution modes. Auto-ranging is accomplished by observing magnetometer output over one rotation of the spacecraft and setting range change decisions which are implemented by the instrument synchronously with the telemetry stream to avoid ambiguity in telemetered data. Either of the two axes in the spin plane may be selected by ground command to control auto-ranging of the instrument.

3.5. Magnetometer boom

Magnetometers in space flight often suffer severe degradation from the effects of fixed and variable spacecraft magnetic fields. For complex spacecraft the only satisfactory solution is to place the sensor on a long extendable boom. Both DE spacecraft incorporate 6 m magnetometer booms. The resulting field at the sensor is less than 1 nT from all spacecraft sources. Figure 3 is a photograph of the DE-A magnetometer sensor mounted to the boom during magnetic testing at the Goddard Space Flight Center. The magnetometer electronics are mounted in the spacecraft body and connected to the sensor by a cable routed in three equal bundles along the boom longerons to minimize boom stress due to the cable. The booms were extensively calibrated through more than eighteen deployment cycles to develop confidence in their repeatability and to develop the matrix required to transform the measured data to the spacecraft coordinate system. Boom stability is even more important than absolute alignment; short term stability of 0.01 deg is desired for quantitative determination of field-aligned currents. The booms are expected to exceed the requirement of 0.1 deg long term and 0.01 deg short term stability placed on them. Although the boom deployment repeatability was specified to be within ± 0.25 deg, ground test data indicate that deployment repeatability approaching 0.1 deg will be attained.

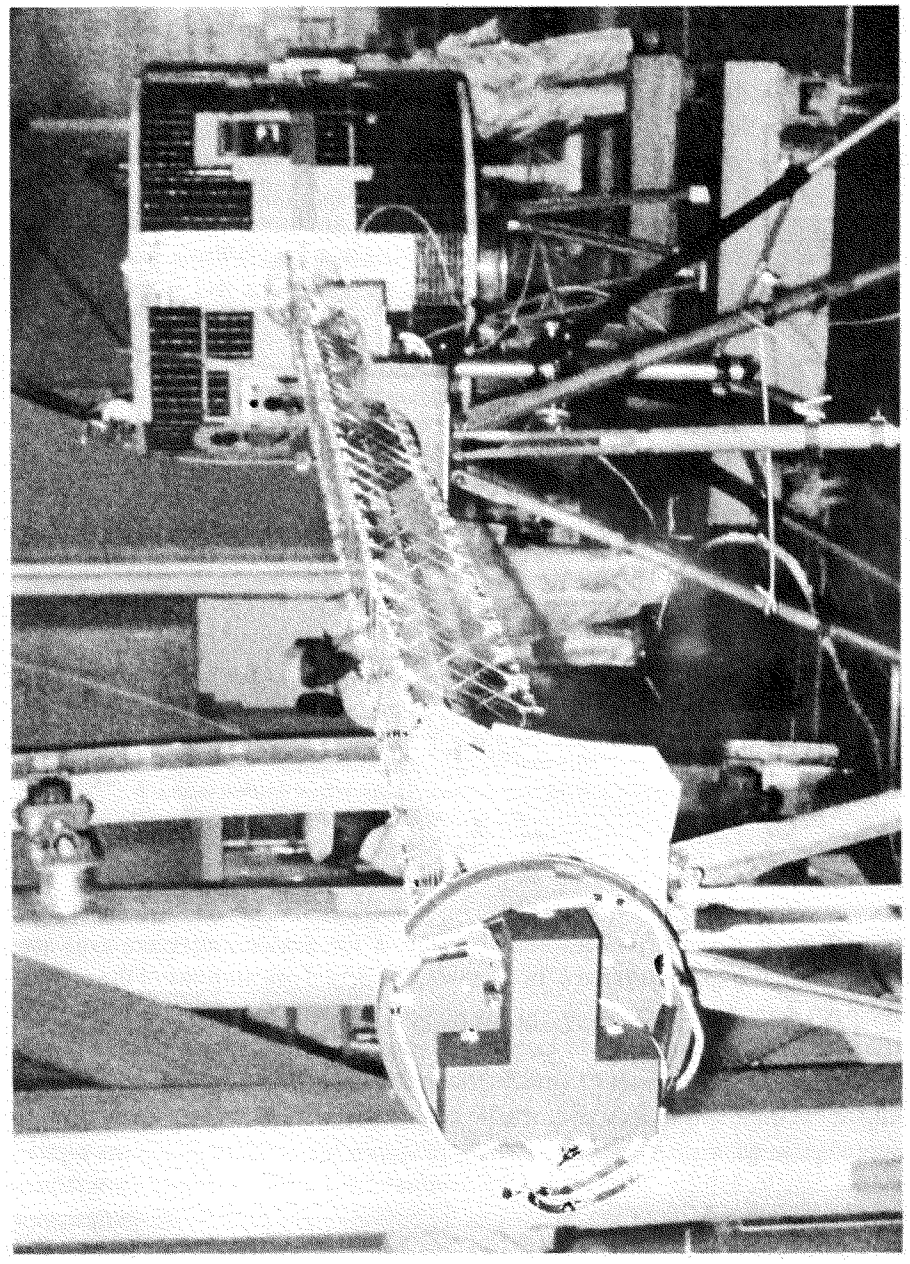

Fig. 3. The sensor mounted to the Astromast. Deployment energy is stored in the coiled longerons of the boom structure. A motor-lanyard combination controls the rate of deployment to 1 foot per minute.

3.6 Sensor orientation

Figure 4 shows the nominal orientation of the magnetometer sensor axes (with subscript, m) relative to the spacecraft axes (with subscript, s). For both spacecraft the sensor z-axis is antiparallel to the spacecraft z-axis. Since this axis is oriented nearly in the east-west direction in orbit, it will be most affected by field-aligned sheet currents at high latitudes. For DE-B, the x-axis is oriented along the velocity vector and will sense primarily the north-south component of the field. The Y-axis for DE-B is roughly earth-pointing and so will sense the local vertical field in the normale mode of spacecraft flight. The DE-B spacecraft will occasionally be placed in a 1 rpm body spin mode which will facilitate

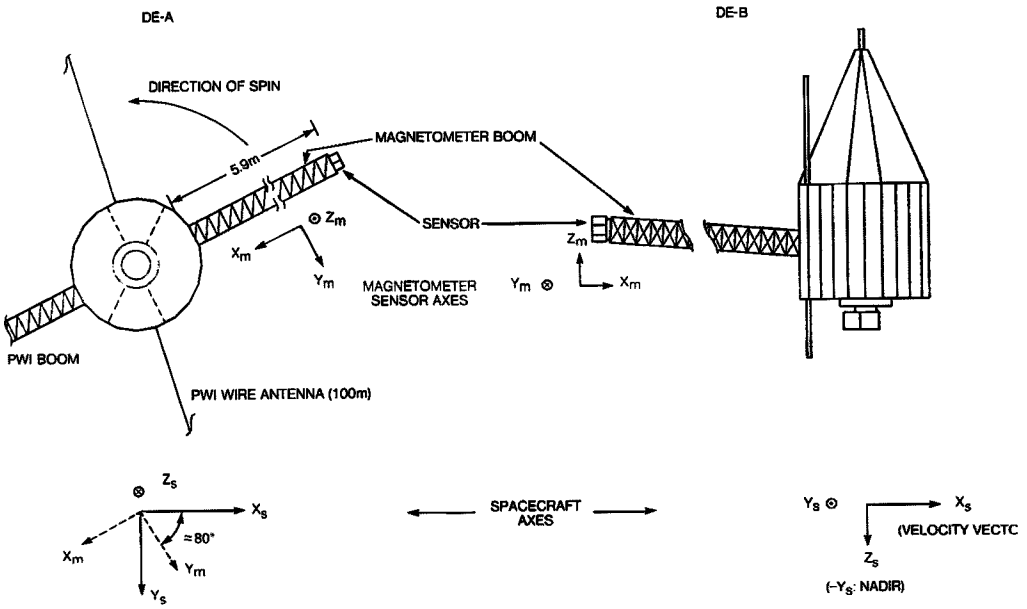

Fig. 4. Sensor orientations for the DE-A and -B magnetometers.

in-flight verification of sensor calibrations. For DE-A the sensor transverse axes are rotated away from the spacecraft axes. In all cases, the actual orientations of the sensor axes have been determined accurately on the ground and will be used in constructing the matrices for transforming data to earth oriented coordinate systems. The accurate vector field model developed from Magsat [6] should make possible in-flight verification of this alignment data and in fact, may enable elimination of biases that remain due to boom mits-alignment.

3.7. Instrument background

The digital fluxgate magnetometer was first used by the Goddard Space Flight Center team on the OGO-5 [7] and ATS-5 [8] at lower dynamic ranges than in the present instrument. Digital fluxgates of this type were also flown on sounding rockets from DEW Line sites [9]. The sensors flown on the SCATHA satellite P78-2 had a similar design

except that the instrument had no digital current compensation. The DE magnetometers borrow from the heritage of all of these predecessor instruments, but require improved stability and accuracy of the digital current sources and improved sensor stability to extend the dynamic range to ±62 000 nT. The DE-A magnetometer is the first instrument to combine digital current sources with range switching to achieve both high precision over wide dynamic range and very high resolution at fields appropriate to DE-A apogee. A hybrid, digital-analog approach was also used in the Magsat vector magnetometer built by Acuna at the Goddard Space Flight Center [10]. In that instrument the digital and analog feedback signals were added electronically before application to a single sense/feedback winding. The Magsat mission provided the only precise global survey of the earth's vector magnetic field that has been accomplished to date. A summary of the DE instrument characteristics is given in Table I.

TABLE I

Instrument characteristics

Instrument:	Triaxial fluxgate magnetometer
Dynamic range:	±62 000 nT
Compensation:	Digitally controlled in 8000 nT steps
	110 nT steps (DE-A only)
Analog dynamic range:	±6000 nT
	±1000 nT (DE-A only)
	± 80 nT (DE-A only)
Resolution:	±1.5 nT
	±0.25 nT (DE-A only)
	±20 pT (DE-A only)
Frequency response:	DC to 25 Hz
Absolute accuracy:	±0.01° ±4 nT (constant temperature)
Temperature coefficient of sensitivity:	30 ppm $°C^{-1}$
Thermal control:	Active heater, passive multilayer insulation
Sample rate:	16 vector samples per second
Power consumption:	3.5 W instrument
	0.6 W thermal control
Weight:	Electronics 3.6 kg
	Sensor 0.9 kg

4. Data Processing

The telemetered sensor readings are converted into components of the magnetic field in the effective sensor coordinate system in which the calibration constants are defined. Temperature corrections on these calibration constants are made by using telemetered temperature readings. However, because of the thermal control of the sensors the temperature corrections are expected to be very small. The magnetic field data in the effective sensor coordinate system are transformed into the three orthogonal components of the spacecraft coordinate system. By incorporating the spacecraft orbit/attitude data, the field components in spacecraft coordinates are transformed into those in various geophysical coordinates. The latter coordinates include topographic (or geographic) and

geomagnetic dipole coordinates. For correlative studies with the solar wind data, solar magnetospheric coordinates [11] or solar magnetic coordinates [12] will also be used.

Plots of the z component in effective sensor coordinates without the temperature corrections provide a quick diagnostic means of finding the presence of high-latitude field-aligned currents because this component is approximately in the east-west direction. For the Mission Analysis File [13], 0.5 s averages of the magnetic field components in topographic and geomagnetic coordinates will constitute the basic data sets. Plots of data at higher sampling rates will be prepared for specific data analyses such as the study of magnetic pulsations, rapid transient variations, or structures in field-aligned currents.

The magnetic field data will also be used for interpretations of data obtained by other DE experiments. The electric field observations by VEFI [14] on DE-B require the magnetic field data to remove the $\mathbf{V} \times \mathbf{B}$ electric field, where $\mathbf{V}$ is the orbital velocity of the spacecraft and $\mathbf{B}$, the magnetic field intensity. All suprathermal particle observations on both spacecraft [13] will require the observed magnetic field direction to deduce the pitch angle distribution of the particles detected.

Acknowledgments

Among the many persons who have made significant contributions to the DE magnetometers, special credit must be given to W. C. Folz for contributions to the electronics design and to S. W. Billingsley for sensor and electronics design. Ralph Ricucci spent many days in test and calibration of the instruments. Appreciation is due C. A. Harris and R. L. Bender of the Environmental Test and Integration Branch at Goddard Space Flight Center for the support of the Magnetic Test Facility and to personnel of the Optical Test Section under Richard Harner for optical test support. The instruments were fabricated for GSFC by Quanta Systems, Inc. under the technical direction of P. Roney. The booms were fabricated for RCA Astro-Electronics by Astro Research Corporation.

References

1. Marshall, S.: *IEEE Transactions on Magnetics* MAG-**3**, 459 (1967).
2. Primdahl, F.: *IEEE Transactions on Magnetics* Mag-**6**, 376 (1970).
3. Ness, N. F.: *Space Sci. Rev.* **11**, 459 (1970).
4. Scouten, D.: *IEEE Transactions on Magnetics* MAG-**8**, 223 (1972).
5. Gordon, D. I., Lundsten, R. H., and Chiarodo, R. A.: *IEEE Transactions on Magnetics* MAG-**1**, 330 (1965).
6. Langel, R., Mead, G., and Lancaster, E.: *Geophys. Res. Letters* **7**, 793 (1980).
7. Ledley, B. G.: *Rev. Phys. Appl.* **5**, 164 (1970).
8. Skillman, T. L.: *NASA Technical Note*, NASA TN D-7496 (1974).
9. Ledley, B. G. and Farthing, W. H.: *J. Geophys. Res.* **79**, 3124 (1974).
10. Acuna, M. H.: *Johns Hopkins APL Technical Digest* **1**, 210 (1980) and references therein.
11. Ness, N. F.: *J. Geophys. Res.* **70**, 2989 (1965).
12. Fairfield, D. H. and Ness, N. F.: *J. Geophys. Res.* **72**, 2379 (1967).
13. Hoffman, R. A., Hogan, G. D., and Maehl, R. C.: *Space Sci. Instrum.* **5**, 349 (1981) (this issue).
14. Maynard, N. C., Bielecki, E. A., and Burdick, H. F.: *Space Sci. Instrum.* **5**, 523 (1981) (this issue).